Investigation of Reciprocating Conformal Contact of Piston Skirt and Ring-pack to Cylinder Liner Under Transient Condition

S. Balakrishnan[1], S. Howell-Smith[2], R, H. Rahnejat[1] and D. Dowson[3]
[1] Wolfson School,
Loughborough University
Loughborough

[2] Perfect Bore Ltd.,
Mayfield Industrial Park,
Weyhill, Andover
Hampshire

[3] Visiting Professor,
Wolfson School, Loughborough University
Loughborough

Abstract

This paper presents an investigation of piston lubrication combining the ring pack in order to study if sufficient lubricant film is formed during reversal at TDC and combustion.

1- Introduction

The piston assembly accounts for approximately 45-60% of the mechanical and frictional losses in internal combustion engines. It is, therefore, essential to minimize this and consequently increase overall efficiency. The automotive industry's key concerns regarding engines are twofold; improving engine efficiency (by producing higher *BMEP*-Brake Mean Effective Pressure) and by increasing *IMEP* (Indicated mean effective pressure) and reducing *FMEP* (Frictional Mean Effective Pressure) , whilst reduction of CO_2, NO_2, *PM* and SO_2 in exhaust gas in accordance with the Government regulations.

The lubricant ingression into the combustion chamber (i.e. reverse blow-by) contributes to particulate emission (*PM*) by as much as 50% (Hofbauer, (2002)), depending on the operating cycle of the engine. Reverse blow-by is not the only reason for oil consumption, which is also affected by evaporation, scraping atomisation, PCV recirculation, squeezing effect, and gas dragging by the ring grooves. These effects are not included in the current analysis. As engines become lighter, with higher combustion pressures, the relative lack of component structural stiffness (brought about by the drive for lowered inertial and driven mass) leads to a poor sealing mechanism, thereby reducing the conformity of ring / piston to bore contact.

Structural integrity problems have been accentuated, as well as those of lubrication and thermal distortion in the cylinder-head and engine block, piston assembly and ring pack (Offner *et al* (2001)). The use of lighter aluminum alloy components tends to increase distortion under high thermal loading, or sometimes they deform permanently under very high and misaligned contact of the load bearing surfaces. The sealing of the ring pack is compromised with thermal distortion of the bore (usually at higher specific output), thereby reducing radial contact conformity. The solution for poor lubrication, potential scuffing and wear is currently sought by the introduction of hard-wearing engineered surfaces.

Improved sealing of the rings translates to a reduced level of oil leakage into the combustion chamber. This is achieved at the expense of an increase in friction between the ring face and the bore/liner, contributing to *parasitic losses* (Taylor *et al* (1998)). In high performance engines, some improvements have been observed (in reduction of *FMEP*) by introducing surface features, such as laser-etched grooves on the liner surface.

This paper aims at providing the insight to the physics of the lubricated conjunction between the piston-skirt and ring pack and the cylinder liner under transient condition using Effective-Influence-Newton Raphson (EIN) as shown by Jalali *et al* (1998).

2- Theoretical Formulation

The formulation comprises two sections: three degrees of freedom dynamics of the piston assembly and transient elastohydrodynamic lubrication of the piston skirt and ring-pack to cylinder liner.

2.1- Dynamics of piston axial, lateral and titling motions

Figure 1 below is a free-body diagram of forces involved in the dynamics of piston-connecting rod-crank system. The three degrees of freedom motion is indicated in the figure. The effective combustion gas force, f_g is applied in an eccentric position with respect to the gudgeon pin centre: C_p, and the centre of gravity of the piston assembly is also away from the pin centre, indicated by C_g. The force and moment equations are obtained as (Xie *et al* (1998)):

$$f_z = f_{ip} + f_{ig} + f_{r2} - f_{r1} - f_{con}\sin\phi \quad (1)$$

$$f_x = f_{gp} + f_{gg} + f_g - f_{con}\cos\phi \quad (2)$$

$$\begin{aligned} m_z &= f_{ip}(a-b) + (f_g \times C_g) \\ &-(f_{gp} \times C_p) + m_c + m_{fr1} + m_{fr2} \end{aligned} \quad (3)$$

The inertial forces and moment caused by the secondary motion of the piston (Xie *et al* (1998)) can be expressed as:

$$f_{ip} = m_p\left(\ddot{e}_t + \frac{b}{p_l}(\ddot{e}_t - \ddot{e}_b)\right) \quad (4)$$

$$f_{ig} = m_g\left(\ddot{e}_t + \frac{a}{p_l}(\ddot{e}_b - \ddot{e}_t)\right) \quad (5)$$

$$m_c = \frac{I_p}{p_l}(\ddot{e}_t - \ddot{e}_b) \quad (6)$$

Equation (1) and (2) be re-written in terms of the connecting rod force, f_{con}, and then substituted into equation (1) to yield the kinetic balance in the direction of the approach of the contiguous bodies in contact (i.e. the z-direction in figure 1) as:

$$\begin{aligned} f_z &= f_{ip} + f_{ig} + f_{r2} - f_{r1} \\ &-\tan\phi(f_{gp} + f_{gg} + f_g) \end{aligned} \quad (7)$$

The various force components in the vertical direction can be lumped together to simplify the above equation set and yield the following expressions:

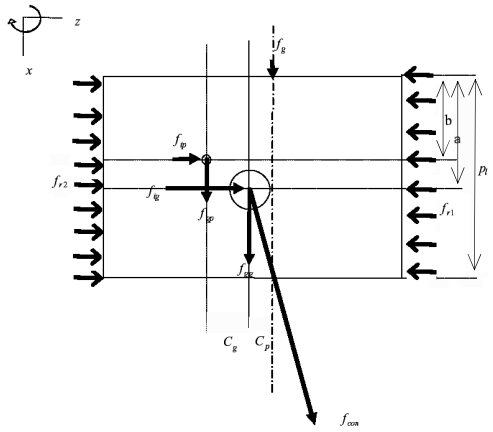

Figure 1: Free-body diagram of forces on the piston

$$m_s + m_{fr1} + m_{fr2} = -m_c - f_{ip}(a-b) \quad (8)$$

$$f_s = f_{ip} + f_{ig} + f_{r2} - f_{r1} \quad (9)$$

where:

$m_s = (f_g \times C_g) - (f_{gp} \times C_p)$ and

$f_s = \tan\phi(f_{gp} + f_{gg} + f_g)$.

Now substituting for the inertial forces and moment into equations (8) and (9), the system dynamics can be represented by the following:

$$\begin{bmatrix} m_g\left(1-\frac{a}{p_l}\right) + m_p\left(1-\frac{b}{p_l}\right) & m_g\frac{a}{p_l} + m_p\frac{b}{p_l} \\ \frac{I_p}{p_l} + m_p(a-b)\left(1-\frac{b}{p_l}\right) & m_p(a-b)\frac{b}{p_l} - \frac{I_p}{p_l} \end{bmatrix} \begin{bmatrix} \ddot{e}_t \\ \ddot{e}_b \end{bmatrix} = \begin{bmatrix} f_{r1} + f_{r2} + f_s \\ m_{fr1} + m_{fr2} + m_s \end{bmatrix} \quad (10)$$

Where, referring to figure 1, using geometric relationships, the tilt of piston, β and the lateral

motion e_l, can be substituted by deviation of top of piston, e_t, and the deviation of the bottom of the piston, e_b from the centre-line axis. This is written as:

$$e_t = e_l + a\beta \tag{11}$$

$$e_b = e_l - (p_l - a)\beta \tag{12}$$

In the current analysis the effect of moment loads due to lubricated contact have been ignored, thus: $m_{fr1} = m_{fr2} = 0$.

Therefore, equation (10) provides the combined lateral and tilting motions of the piston. The axial motion is kinematic (i.e. pre-determined by the relationship between the crank rotation and piston motion). This is obtained in terms of the various engine order response characteristics of the engine, in this case up to and including the 8th engine order, thus:

$$\dot{x} = r\sin\omega t - \Psi_i \cos(2i-1)\omega t + \Psi_{i-1}\sin 2i\omega t \tag{13}$$

where $i = 1 \rightarrow 4$ and $\Psi_i = f(r, l, C_p)$ (see Balakrishnan (2002)). The connecting rod length, l and the crank radius, r is 105 mm and 22.14 mm respectively.

Frictional moment in the wrist pin bearing would also play a small role in tilting motion of the piston due to very small angles of tilt, and is ignored in the current analysis. This effect has been taken into account by other research workers, such as (Dursunkaya and Keribar (1992)).

2.2- Transient lubricated contact

There are 6 potential contact configurations in the transient motion of the piston against the cylinder liner in the case of the 10 cylinder high performance Formula 1 (F1) engine considered in this paper. These include the piston skirt contacts with the major and minor thrust and the corresponding contacts made by the two piston rings: the oil control ring and the compression ring, again with the two thrust sides. Clearly, the contact conditions are worst in most instances on the major thrust side. Nevertheless, unlike other analyses reported in the literature all the above contacts have been included in the analysis.

The solution involves the treatment of contacts with the major or minor thrust sides to include in each case the profile of the piston skirt and all rings. This yields a very long contact area on each side, necessitating many mesh point calculations, which is computationally very CPU time intensive and requires a large storage capability. However, the alternative would be to determine the inlet boundary conditions in each step of time for the piston skirt or the ring pack (depending on the direction of entraining motion) which would depend on the prevailing outlet conditions induced by the other rings. This would require the determination of the film thickness at the outlet of any of the above mentioned contacts and the determination of surface tension effect to replenish the inlet meniscus for the following contact. Such an approach would render an even more complex and time consuming analysis.

In the current solution, the ring pack is assumed not to move with respect to the piston. This assumption means that equilibrium condition is assumed for axial freedom of rings, the repercussion being that ring flutter which occurs in practice is ignored. However, it is acknowledged that oil leakage can be reduced under certain circumstances by ring flutter at specific positions during the stroke. The stiffness of the ring is included in the model, which leads to its global deformation being included in the analysis, as well as clearly the local deformation due to the generated contact pressures. However, other ring motion such as flutter or twist are not included, but indeed do occur, which undoubtedly do affect lubrication. The solution for each extended contact (one with the major thrust side and the other with the minor thrust side) is obtained by the combined solution of Reynolds equation, the elastic film shape and the lubricant state equations for the bulk characteristic rheological behaviour of the lubricant (i.e. viscosity and density). It should also be noted that the solutions provided in this paper pertain to isothermal conditions. This assumption can also have serious shortcomings, since thermal distortion of the partial piston skirt, particularly in these high performance motorsport engines, is expected to play a role, as investigated by Balakrishnan (2002).

The Reynolds equation for transient analysis is given as:

$$\frac{\partial}{\partial x}\left(\frac{\rho h^3}{\eta}\frac{\partial p}{\partial x}\right)+\frac{\partial}{\partial y}\left(\frac{\rho h^3}{\eta}\frac{\partial p}{\partial y}\right)= 12\left(u_{AV}\frac{\partial}{\partial x}(\rho h)+v_{AV}\frac{\partial}{\partial y}(\rho h)+\frac{\partial}{\partial t}(\rho h)\right) \quad (14)$$

The final term on the right hand side provides the squeeze film velocity at any instance of time and at any given location within the contact due to the mutual approach or separation of the contiguous solids in combined rigid body motion and rate of change of deformation of the mating bodies. Transient conditions in many applications occur as the result of this squeeze film action, such as in bearings running with constant rotational velocity, but being subjected to cyclic loading or indeed having insufficient preload or interference fitting, thus suffering from the emergence of loaded and unloaded regions. In the case of piston lubrication, there is additional transience due to changes in the entraining speed:

$$u_{av}=\frac{1}{2}(u_b+u_p)=\frac{1}{2}\frac{dx}{dt}=\frac{\dot{x}}{2},$$

where $u_b=0$.

Additionally, with the assumption of no side-leakage in the contact: $v_{av}=0$. Also note that *x* in the Reynolds equation represents the unwrapped circumferential contact, or: $y=r\varphi$.

Solving Reynolds equation in the form given above for a conforming contact as that of piston against cylinder liner or bore necessitates that the gap at the edges of the contact, as determined by an equivalent solid of revolution of radius, R_x remains the same as the original clearance, *C*. Thus: $r_{by}=r_{py}+c$, and: $R_y=\frac{r_{py}(r_{py}+c)}{c}$.

The maximum diameter of the piston in the engine under consideration is 94.95 mm, with minimum cold radial clearance of approximately 57.5 μm. The clearance is affected by piston ovality (out-of-roundness), which is included in the model. The radii of curvature in the axial direction are very large indeed, except that the piston skirt has relief radii at its extremities in order to reduce the edge stress concentration, which is typical of contacts of unblended finite length bodies, such as in the non-conforming finite line contact of a roller against a flat (see Kushwaha *et al*, 2002). Since the axial radius of curvature of the bore is extremely large, then in the axial direction: $R_x=r_{px}$, this being typically in the range 500-3000m. These conditions lead to a large rectangular-type contact area (when viewed as unwrapped), particularly with the piston at mid-span location in its reciprocating cycle. The contact area shrinks with low load and cessation of entraining motion at Top Dead Centre (TDC) and Bottom Dead Centre (BDC), but is normally still large enough to deviate significantly from semi-infinite elastic conditions that form the basis of the classical Hertzian theory. Thus, calculation of contact deflection cannot be based on classical theory, and should be computed from basic principles.

The elastic film shape is obtained as:

$$h_{i,j}=s_{t_{i,j}}+\delta_{z_{i,j}}+h_0 \quad (15)$$

where originally: $h_0=C$, and the tilted (misaligned) profile is obtained at any instant of time as:

$$s_{t_{i,j}}=s_{i,j}+\Delta x\left(i-n_{gx}\right)\tan\beta \quad (16)$$

where for a crowned or barrel-shaped piston:

$$s_{i,j}=\frac{\left(x_{i,j}-m\right)^2}{2R_x}+\frac{\left(y_{i,j}-n\right)^2}{2R_y} \quad (17)$$

The contact deflection is obtained, using:

$$\delta_{z_{i,j}}=\frac{2p_{i,j}}{\pi E'}\int_{-\tilde{a}}^{\tilde{a}}\int_{-\tilde{b}}^{\tilde{b}}\left\{\frac{dx_1dy_1}{\left[\left(y-y_1\right)^2+\left(x-x_1\right)^2\right]^{1/2}}\right\} =\frac{2p_{i,j}}{\pi E'}D^* \quad (18)$$

for a rectangular contact area of $2\tilde{a},2\tilde{b}$, where:

$$D^*=\left(x+\tilde{b}\right)\ln\frac{(y+\tilde{a})+\left[(y+\tilde{a})^2+\left(x+\tilde{b}\right)^2\right]^{\frac{1}{2}}}{(y-\tilde{a})+\left[(y-\tilde{a})^2+\left(x+\tilde{b}\right)^2\right]^{\frac{1}{2}}}+(y+\tilde{a})\ln\frac{\left(x+\tilde{b}\right)+\left[(y+\tilde{a})^2+\left(x+\tilde{b}\right)^2\right]^{\frac{1}{2}}}{\left(x-\tilde{b}\right)+\left[(y+\tilde{a})^2+\left(x-\tilde{b}\right)^2\right]^{\frac{1}{2}}}$$
$$+\left(x-\tilde{b}\right)\ln\frac{(y-\tilde{a})+\left[(y-\tilde{a})^2+\left(x-\tilde{b}\right)^2\right]^{\frac{1}{2}}}{(y+\tilde{a})+\left[(y+\tilde{a})^2+\left(x-\tilde{b}\right)^2\right]^{\frac{1}{2}}}+(y-\tilde{a})\ln\frac{\left(x-\tilde{b}\right)+\left[(y-\tilde{a})^2+\left(x-\tilde{b}\right)^2\right]^{\frac{1}{2}}}{\left(x+\tilde{b}\right)+\left[(y-\tilde{a})^2+\left(x+\tilde{b}\right)^2\right]^{\frac{1}{2}}}$$

The analysis reported later indicates that for the current piston profile and loading condition, iso-viscous rigid conditions dominate for most of the cycle. However, in the vicinity of the maximum combustion pressure, iso-viscous elastic conditions are noted, and precisely for this reason it is inappropriate to undertake a purely hydrodynamic analysis, and it is difficult to predict the boundary between these conditions during the cycle, in order to save on computational time. It should also be noted that thermal distortion of the piston is not included in the current analysis. Its inclusion would lead to reduced clearance which can promote elasto-hydrodynamic conditions, with higher pressures than those observed here.

The lubricant state equations are given as follows:

For viscosity-pressure dependence according to Roelands (1966):

$$\bar{\eta} = \frac{\eta}{\eta_0} = \exp^{(\ln \eta_o + 9.67)\left(-1+\left(1+5.1\times10^{-9}\, p\right)\right)} \quad (19)$$

And for density-pressure behaviour by Dowson and Higginson (1966) as:

$$\bar{\rho} = \frac{\rho}{\rho_0} = 1 + \frac{0.6\,p}{1+1.7\,p} \quad (20)$$

The inlet alters from the bottom end of the piston skirt to its top edge beyond the top ring as the piston axial motion reverses at the TDC. The outlet boundary condition used is that of Reynolds: $p = \frac{dp}{dx} = \frac{dp}{dy} = 0$.

3- Method of solution

The inertial dynamics outlined in section 2.1 are solved in order to obtain the values $\ddot{e}_t$, $\ddot{e}_b$ and β. A step-by-step integration algorithm, based upon the Newmark β integration technique (linear acceleration method) is used to obtain the values of e_t and e_b. These values, together with β and $|\dot{x}|$ are required for the determination of the lubrication condition , as outlined in section 2.2. At any step of time, the contact pressure distribution and film shape for both contacts with the major and minor thrust sides are determined. Then, the corresponding contact forces are obtained as the integrated pressure distributions:

$$f_{rk} = \int_i \int_j p_{ij}\, dx dy, \; k = 1,2 \quad (21)$$

These values are then passed back to the procedure mentioned in section 2.1 for the next step in the inertial dynamic analysis. It should be noted that moment calculations $m_{frk}, k = 1,2$ are ignored in the current analysis to save on the computation time in this initial analysis, but can clearly be included.

The convergence criteria for inertial dynamics are set at:

$$\left|\frac{\ddot{e}_{t,n} - \ddot{e}_{t,n-1}}{\ddot{e}_{t,n}} \mathrm{X}100\right| < 1$$
$$\left|\frac{\ddot{e}_{b,n} - \ddot{e}_{b,n-1}}{\ddot{e}_{b,n}} \mathrm{X}100\right| < 1 \quad (22)$$

where *n* is the time step index.

The solution for transient lubricated contacts is based on the Effective Influence Newton-Raphson method (EIN), the full description of which is available in Jalali *et al* (1998) and Balakrishnan (2002). Briefly, the Reynolds equation is discretized over a grid of $n_x \mathrm{X} n_y$ by finite differences and represented in the form:

$$\sum_{k=2}^{nx-1} \sum_{l=2}^{ny-1} \left[J_{(ij,kl)} \right] \cdot \Delta p_{(k,l)} = -f^R{}_{(i,j)} \quad (23)$$

where the residual function $f^R(i,j)$ is the Reynolds equation itself and the Jacobian matrix contains the terms: $J_{(ij,kl)} = \partial f^J{}_{(i,j)} \big/ \partial \bar{p}_{k,l}$. The discretised forms of the Residual function $f^R(i,j)$ and the Jacobian function $f^J(i,j)$ (also the Reynolds equation with different discretization of the Couette flow terms to that of $f^R(i,j)$) can be found in Jalali *et al* (1998). The convergence criterion used in the lubrication analysis is based upon generated pressures in

each step of time, n, base on an iteration index n':

$$\left| \frac{p_{i,j}^{n'} - p_{i,j}^{n'-1}}{p_{i,j}^{n'}} \right| \leq 0.1 \qquad (24)$$

Therefore, for any time step, indicated by the index *n*, there may be many iterations of the contact calculations, denoted by the index *n'*. The inertial dynamics itself is subjected to many iterations within each step of time, denoted by the index *n*.

The initial conditions must be set to start the calculation process. This is set at a position close to the TDC and on the upstroke cycle of piston motion. At such a location the value of $|\dot{x}|$ can easily be determined from the kinematic equation (13), and assuming steady state entraining motion, the lubrication conditions can be obtained and the contact forces evaluated, leading to the first time determination of the inertial dynamics of the system. Subsequent iterations alter the assumption of pure entraining motion. It should also be noted that the problem at hand is not an initial value one. A position near to TDC is used, as it serves two purposes. Firstly, the piston tilt is almost completely to the major thrust side, and with the initial clearance taken into account the tilted geometry of the contact is simple to evaluate, using the geometrical relations in section 2.1. Secondly, with the purpose of analysis being the investigation of transient behaviour of the contacts in reversal, the required computational steps are considerably reduced.
The simulation study commences from a position prior to the TDC (sufficient number of time steps away from the TDC to reduce the transient effect of imposed initial conditions) on the piston upstroke, through cessation of motion at TDC and reversal to the downward stroke and through the maximum combustion force.

4- Simulation results

A tribodynamic analysis of a piston-connecting rod-crank sub-system of a 10-cylinder, 4-stroke, V10, 2.997 Litre engine as typically used in Formula 1 motorsport. The combustion pressure, unlike the conventional spark ignition engine, is 12 MPa, occurring during the piston cycle, 11° past the TDC, as measured in terms of the crank-angle rotation.

The profile of the piston-skirt and the ring-pack is shown in figure 2. The left-hand side of the figure represents the bottom side of the piston skirt. The piston rings are shown beyond the skirt's top side relief radius. The length of piston skirt is 33 mm including oil grooves and ring lands. The piston gudgeon pin is offset by 10 μm. The piston profile in the circumferential direction is, in fact, oval. The longitudinal profile of the piston skirt incorporates relief radii at its axial extremities. The piston skirt axial profile is asymmetrical, with the top and bottom end sections having radii that deviate from the principal nominal radius by 80 μm on the top and 46 μm at the bottom. The bottom section is merely a chamfer. This chamfer creates the wedge effect for lubricant entrainment as the piston traverses toward the BDC.

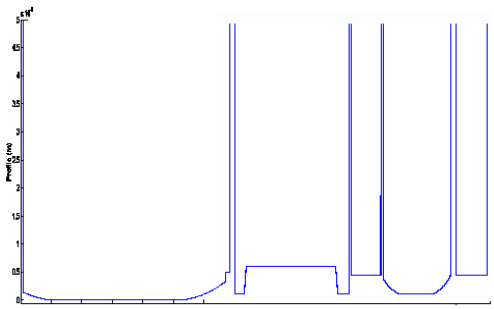

Figure 2: Profile of piston skirt and rings

The actual profile, shown in figure 2 represents an aligned conforming profile of the skirt against the cylinder bore.

The contact domain is quite large in many instances and in order to obtain convergence and realistic pressure distributions, it is necessary to use as refined a computational mesh as possible. A mesh of 1800 by 180 nodes (the former in the axial direction, i.e. along the length of the sliding contact) is used in this analysis. This can be seen in the three dimensional pressure distribution of figure 3, which is for the position of TDC, with the maximum combustion pressure, where the downward sliding velocity of the piston is 1.9 m/s.

Note that pressure is generated over 180 circumferential elements (360 elements are used for a 2π contact).

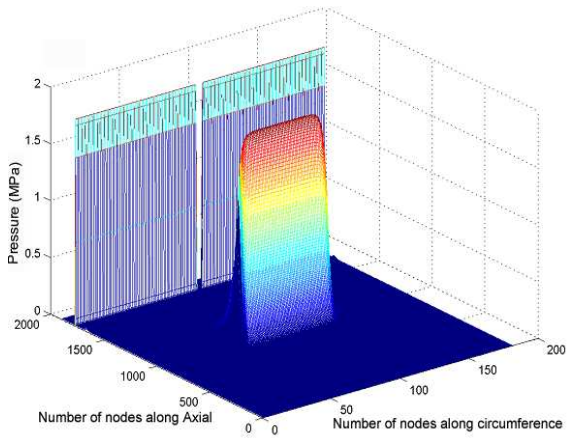

Figure 3: 3D Pressure distribution on the major thrust side at TDC

The first area of pressure rise on the right-hand side of the figure corresponds to the piston skirt contact, followed by a very small rise in pressure on the oil control ring, and very steep pressure rise over the top ring (i.e. the compression ring). On the skirt the pressures peak to a value of approximately 1.2 MPa for the total contact load of 0.5 KN. The low pressures are due to the very large conforming contact and in the case of the piston skirt are not in excess of the maximum pressures experienced by commercial diesel engines.

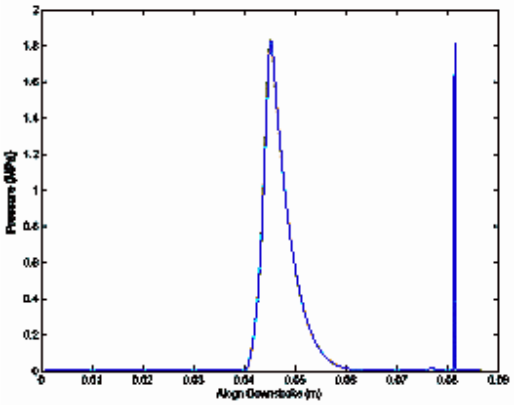

Figure 4 Central contact pressure distribution at maximum combustion pressure

At the maximum combustion position (11° past TDC), the contact load increases to nearly 6 KN, but the rise in pressure is less pronounced. This is because the tilt of the piston toward the major thrust side is reduced, and therefore the area of contact is increased. The pressure distribution on the major thrust side is shown in figure 4. Here the small pressures generated on the oil control ring can be seen in between the two pressure profiles: the one on the left hand side representing the piston skirt and the other on the right hand side the compression ring.

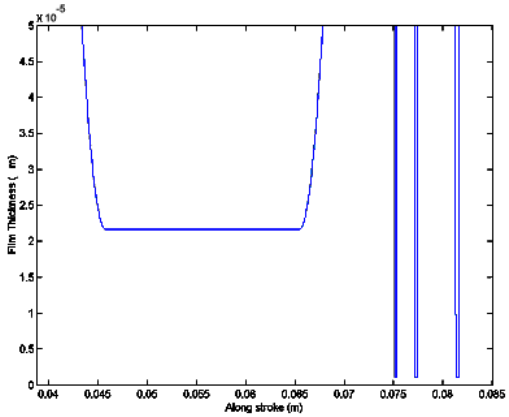

Figure 5 Central film thickness corresponding to figure 4

Finally, figure 5 shows the film shape along the contact at the maximum combustion (corresponding to the pressure distribution in figure 4). This can be related to the contact profile in figure 2 noting that the radial clearance of 57.5 μm is used. With a fully flooded inlet assumed ahead of the piston skirt in the downward sense of the piston, there is plentiful supply of lubricant, and with a large contact area and the use of very high relief radii generation of high pressures is inhibited. Therefore, the conditions are iso-viscous rigid and a film of approximately 20 μm over the skirt is obtained. The same favourable conditions are not obtained over the piston ring-pack to cylinder liner contacts, where the predicted films are approximately 1-2 μm, which with thermal expansion (not taken to account here) and ring flutter, may in some circumstances, lead to scuffing of the cylinder liner. It is easy to envisage that in the upstroke sense of the piston, where the inlet boundary to the piston skirt contact is determined by the outlet films of the rings, scuffing of the piston skirt can also take place due to insufficient supply of lubricant. Therefore, more realistic analysis of the contact is required to include thermal distortion, as well as realistic inlet boundary conditions as opposed to the fully flooded assumption.

5- Conclusion

The results indicate that a coherent lubricant film would exist during the piston cycle with the

radial clearance of 57.5 μm. The composite RMS value of the cylinder liner and piston ring roughness is approximately 0.1-0.2 μm. With the smallest film thickness predicted above 1 μm, scuffing failure appears unlikely. However, scuff marks have been observed at both TDC and BDC, indicating that the predicted films are greater than those achieved in practice. Since iso-viscous rigid regime of lubrication prevails in these localities at low contact loads, it is clear that in practice the designed clearance is breached, possibly by thermal expansion. Therefore, the analysis highlighted in this paper should be extended to include the effect of thermal expansion of the piston and the cylinder liner. Furthermore, the viscosity of the lubricant should be adjusted for the prevailing contact temperature. Finally, a more representative analysis should make use of open boundary conditions to take into account of combustion pressure and the crank pressure on the upstroke and downstroke senses of the piston instead of the Reynolds boundary condition.

Acknowledgements
The authors would like to express their gratitude for financial and technical support of Perfect Bore Motorsport (PMI).

References

Balakrishnan, S. (2002), Transient Elastohydrodynamic Analysis of Piston Skirt Lubricated Contact Under Conbined Axial, Lateral and Tilting Motion, PhD Thesis, Loughborough University, Loughborough, UK.

Dowson, D. and **Higginson, G.R**. (1966), Elastohydrodynamic Lubrication: The Fundamentals of Roller and Gear Lubrication, Pergamon Press, Oxford, UK.

Dursunkaya, Z. and **Keribar, R.** (1992), Simulation of secondary dynamics of articulated and a conventional piston assemblies, SAE pap. No. 920484

Hofbauer, P. (2002): Advanced Diesel Engines for the EU and US Automotive Markets, The United States Energy Association Energy Forum In Conjunction with the G-8 Ministerial Conference Proceedings, Johannesburg

Jalali-Vahid, D, Rahnejat, H and Jin Z.M. (1997): Elastohydrodynamic lubrication of point contact under combined rolling and squeeze film. H Rahnejat and R Whalley (eds), *Tri-Annual Conference on Multi-Body Dynamics: Monitoring and Simulation Techniques*, Mechanical Engineering Publications, London, ISBN 1-86058-064-5

Liu, K., Xie, Y.B. and **Gui, C.L.** (1998): A comprehensive study of the friction and dynamic motion of the piston assembly. *Proc. Institution of Mechanical Engineers Part J*, Volume 212, pp. 221-226

Offner, G. and Priebsch, H.H. (2000): Elastic body contact simulation for predicting piston slap induced noise in an IC engine. in H Rahnejat and R Whalley (eds), *Multi-Body Dynamics: Monitoring and Simulation Techniques-II*, Mechanical Engineering Publications, London, ISBN 1-86058-253-3

Roelands, C.J.A. (1966): Correlation Aspects of Viscosity-Temperature-Pressure Relationship of Lubricating Oils. Ph.D. Thesis, Delft University of Technology, The Netherlands.

Taylor, C.M (1993): Engine Tribology. Tribology Series, Elsevier, Oxford, 26

Notations

a height measured from centre of gudgeon to piston crown (m)

b height of the centre of mass of piston measured from piston crown (m)

$\tilde{a},\tilde{b}$ Computational domain, (m)

C_g offset of centre of mass measured along the z-axis from gudgeon (m)

C_p offset of gudgeon pin from centre line (m)

e_b lateral displacement of lower end of the piston skirt (N)

e_l lateral displacement of gudgeon pin (m)

e_t lateral displacement of upper end of the piston skirt (m)

E' Modulus of elasticity, $\left(N/m^2\right)$

f_{con} connecting rod force (N)

f_g gas force (N)

f_{gg} inertial force of gudgeon due to primary motion (N)

f_{gp} inertial force of piston due to primary motion (N)

f_{ig} inertial force of gudgeon due to secondary motion (N)

f_{ip} inertial force of piston due to secondary (N)

f_{r1} reaction due to lubricant at major thrust side (N)

f_{r2} reaction due to lubricant at minor thrust side (N)

$\bar{h}$ Non-dimensional film

I_p piston inertia about its centre of mass $(kg.m^2)$

m_g mass of gudgeon pin (kg)

m_p mass of gudgeon pin (kg)

m_{fr1}, m_{fr1} hydrodynamic reaction moments, (Nm)

p Applied pressure, $\left(N/m^2\right)$

$\bar{P}$ Non-dimensional pressure

p_l Piston length, (m)

r_{bx} bore radius in the inlet direction, (m)

r_{by} Circumferential radius of bore, (m)

r_{px} Barrel radius of piston, (m)

r_{py} Circumferential radius of piston, (m)

t Time, (s)

x, y, z Cartesian Coordinates

β tilt of piston, (rad)

δ Elastic deformation, (m)

ϕ conrod angle, (rad)

η dynamic viscosity, $(Pa\ s)$

$\bar{\eta}$ Non-dimensional viscosity

η_0 absolute viscosity at $p = 0$ and a constant temperature, $(Pa\ s)$

ρ_0 density at zero pressure

ρ density

$\bar{\rho}$ Non-dimensional density

ω crank angular velocity (rad/s)